Proceedings of the 7th RSI
International Conference on Robotics and Mechatronics (ICRoM 2019)
November 20-21, 2019, Tehran, Iran

Implementation of an improved moment-based visual servoing controller on an industrial robot

Parisa Masnadi Khiabani, Javad Ramezanzadeh and Hamid D. Taghirad, *Senior Member, IEEE*
Advanced Robotics and Automated Systems (ARAS), Industrial Control Center of Excellence (ICCE),
Faculty of Electrical Engineering, K.N. Toosi University of Technology, Tehran, Iran.
Email: p.masnadi@ee.kntu.ac.ir , javadramezanzadeh@gmail.com, taghirad@kntu.ac.ir

***Abstract*—In this paper, robust nonlinear control of moment-based visual servoing has been proposed. Due to the nonlinear nature of system, proportional integral sliding mode controller could improve the performance and robustness of visual servoing. The proposed method not only increases domain of attraction even in extraneous image regions, but also it achieves convergence to the target point despite of uncertainties. The stability of the controller is analyzed by Lyapunov's theorem. Furthermore, Integrated control of 4 DOF camera motions in this work, drastically improves the accuracy in compare with the kernel-based sliding mode visual servoing [1]. Different experiments are done to demonstrate considerable performance improvements on 5 DOF industrial robot.**

***Index Terms*—Image moments, Sliding mode control, visual servoing**

I. Introduction

The aim of visual servoing (VS) is tracking an object, based on the feedback information provided by vision sensor. Achieving a robust, accurate, and quick tracking of featureless objects in the presence of partial disappearing of features, are the main achievements of this paper. The primary approaches in VS had been based on matching simple geometrical features such as coordinates of points, straight lines or ellipses [2], [3]. These methods have been restricted to the limited set of objects. In order to improve the previous tracking methods, in [4] the image space was reduced to the set of eigen space provided by the set of images around the target position in offline mode. Moreover, there were no analytical form for interaction matrix are reported.

In the current paper similar to [5] the moments that may be computed easily from binary images, are considered as visual features. The proposed analytical form of interaction matrix makes a robust analysis of the method possible. Moments considerably are used in computer vision for shape-descriptor purposes [6]. In addition invariant properties of combination of moments make them suitable for pattern recognition purposes [7], [8]. Tahri [9] modified the previous suggested moments to produce better decoupled form of interaction matrix. In the mentioned methods, the linear feedback controller has been designed to control a manipulator's motion. Since there is a nonlinear relation between image space and 3-D position, the linear controllers are able to only stabilize the system locally, and furthermore, the possibility of convergence to a local minima will increase. In [10] the author proposed applying Gaussian masking to image, which set the priority to the central part of the image and decreases smoothly as approaching boarders. The selected features for translation and scale are affected by Gaussian masking and there are no more invariants. Consequently, the modified interaction matrix is more complicated than uniformly weighted moments.

By the same spirit, in [11] the author proposed kernels for VS. Kernels are the weighted image signals and the general form of moments. In this method, each degree of freedom should be controlled separately due to the dependency between suggested kernels which results in longer convergence time. Inspired by [11], in [1], combination of the aforementioned kernels with sliding mode has been proposed. The problem of separately controlling of each DOF is still remained, while tracking performance has been improved and domain of attraction is enlarged.

Conceptually, there is no general analytical method applicable to model an arbitrary nonlinear system. In VS the imperfections are related to the unmolded dynamics, and calibration parameters which lead to uncertainty in interaction matrix components. In our point of view, there are two approaches to deal with the VS nonlinearity, the first one is to shape interaction matrix into diagonal form by selecting proper features, and the second one is to use a nonlinear controller. However, the former method just could lead to decoupled form of interaction matrix as much as possible and it could not deal with uncertainty. The latter method could control the system in spite of nonlinearities and uncertainties.

In this paper, sliding mode controller which is a robust nonlinear controller, in combination with image moments is proposed. This is much more compatible with the nature of system, and moreover, it avoids the complicated process of decoupling nonlinearity in interaction matrix. In order to implement the controller, the proportional-integral (PI) sliding surface has been suggested. The efficiency of proposed controller has been demonstrated by implementing it on a 5 DOF industrial manipulator. The obtained results imply considerable improvements in domain of attraction, tracking error, and convergence rate compare to that reported in [1], [5]. Domain of

978-1-7281-6604-9/19/$31.00 ©2019 IEEE

attraction has been considerably increased, so as convergence to the target point may be achieved even in extraneous image regions, where the object is not completely in camera's field of view. Furthermore, using SMC has noticeably reduced the tracking error, and increased the convergence rate. Another advantage of this work respect to [1] is that four degree of camera motions are controlled simultaneously.

The remainder of this paper is organized as follows: In section II basic definition of image moments is reviewed, then invariants moments are summarized, and finally, the general analytical form of the interaction matrix is given. Section III presents the proposed controller and analyzes the stability of the method. To validate the suggested controller, the experimental results are reported in Section IV. The conclusion is presented in Section V

II. Vision Modeling

A. Moments Representation

One of the feature descriptors which has been widely used in image processing is moment. It simply characterizes an image by reducing its probability distribution function to a sequence of numbers. This is useful in comparing distributions of images numerically. Moments of a positive real bounded function, $f(x,y)$, within a finite region R is defined by [12]

$$m_{p,q}(t) = \iint_{R(t)} f(x,y)x^p y^q dxdy \quad p,q = 0,1,2,... \quad (1)$$

Where $f(x,y)$ is a piece-wise continuous function and has non-zero values on a finite region R in $x-y$ plane. $p+q$ represents the order of the moment. In the image processing, $f(x,y)$ may be considered as image intensities. Using binary images, eq. (1) may be written as follows

$$m_{p,q}(t) = \iint_{\Re} x^p y^q dxdy \qquad p,q = 0,1,2,... \quad (2)$$

in which $\Re$ is the region of image where the object has been projected. In digital images the integral is replaced by summation, and the image moments may be written as follows [9]

$$m_{pq} = \sum_{k=1}^{n} f(x,y)x_k^p y_k^q \quad (3)$$

where $f(x,y)$ is the intensity of binary image which can be set to 0 or 1. x,y are the index of image points in metric coordinates, and n is the number of pixels.

By computing the moments with respect to the object's mass center coordinates the centered moments are obtained. They are defined by

$$\mu_{p,q}(t) = \iint_{\Re} (x-x_g)^p (y-y_g)^q dxdy \quad (4)$$

where $x_g = \frac{m_{10}}{m_{00}}$, $y_g = \frac{m_{01}}{m_{00}}$. The centered moments are invariant to 2-D translational motions. The discrete form of equation (4) may be given as

$$\mu_{pq} = \sum_{k=1}^{n} f(x,y)(x_k - x_g)^p (y_k - y_g)^q \quad (5)$$

Different types of moments or combination of them may be used as invariant to geometric transformation such as translation, scaling, and rotation. This feature has significant steps toward reliable and robust recognition of an object's location, size, and orientation. Several combinations of moments have been proposed for scale invariants. A proper scale invariant which is presented by [9] is as follows.

$$I_s = \frac{m_{p,q}}{m_{00}^{\frac{(p+q+2)}{2}}} \quad (6)$$

In this paper, as same as [9], eq.(6) has been used.

B. Interaction Matrix of Image Moments

The interaction matrix relates the time derivative of image moments, $\dot{m}$, to the instantaneous velocity of the camera as follows [13]

$$\dot{m}_{pq} = \mathbf{L}_{m_{pq}} \mathbf{v} \quad (7)$$

in which, $\mathbf{L}_{m_{pq}}$ is the interaction matrix, and $\mathbf{v}$ is the translational and rotational velocity of camera.

The region $\Re$ is the only time varying part of equation (2); therefore, the derivative of moment can be computed by

$$\dot{m} = \oint_{\mathcal{C}(t)} (x^p y^q) \dot{\mathbf{x}}^T \mathbf{n}\, dl \quad (8)$$

where $\mathcal{C}$ is the contour of $\Re$, $\dot{\mathbf{x}}$ is the velocity of pixel point $\mathrm{x} = (x,y)$ on the contour, $\mathbf{n}$ is the outward-pointing unit normal vector on the $\mathcal{C}$, and dl is a small tangent vector along the contour $\mathcal{C}$ [5].

$\dot{\mathbf{x}}$ is related to camera velocity by well-known equation as bellow

$$\dot{\mathbf{x}} = \mathbf{L}_x v_c \quad (9)$$

where $\mathbf{L}_x$ is

$$\begin{bmatrix} \frac{-1}{Z} & 0 & \frac{x}{Z} & xy & -1-x^2 & y \\ 0 & \frac{-1}{Z} & \frac{y}{Z} & 1+y^2 & -xy & -x \end{bmatrix} \quad (10)$$

where x and y are the coordinates of the any point projected in Image and Z is the depth of the point relative to the camera frame [13] and is defined as below

$$\frac{1}{Z} = Ax + By + C \quad (11)$$

A, B, and C are scalar parameters that describe the orientation of plane.

By substituting equation (9) in equation (8), and applying green theorem, the interaction matrix can be obtained (for more details refer to [5]). As mentioned in [5], [9] for the planar object $A = B = 0$ therefore, the simplified form of interaction matrix is written:

$$\begin{cases} \mathbf{L}_{m_{pq}}^{v_x} = -Cpm_{p-1,q} \\ \mathbf{L}_{m_{pq}}^{v_y} = -Cqm_{p,q-1} \\ \mathbf{L}_{m_{pq}}^{v_z} = C(p+q+2)m_{p,q} \\ \mathbf{L}_{m_{pq}}^{\omega_z} = pm_{p-1,q+1} - qm_{p+1,q-1} \end{cases} \quad (12)$$

This significantly reduces the complexity of the formulation introduced in [5]. It can be understood from (12) that in parallel situation, the moments order up to $p+q$ are sufficient

for L calculation of moment order $p+q$. Here C is equal to $\frac{1}{Z}$ because it is assumed the desired position of the object parallel to the image plane. The Interaction matrix components related to translational motion along x and y decrease the order of moment and also rotational motion around optical axes is independent from depth information. Similarly, if we consider the centered moments defined by (2), we obtain

$$\begin{cases} \mathbf{L}_{\mu_{pq}}^{v_x} = 0 \\ \mathbf{L}_{\mu_{pq}}^{v_y} = 0 \\ \mathbf{L}_{\mu_{pq}}^{v_z} = C(p+q+2)\mu_{p,q} \\ \mathbf{L}_{\mu_{pq}}^{\omega_z} = p\mu_{p-1,q+1} - q\mu_{p+1,q-1} \end{cases} \tag{13}$$

As noticed, interaction matrix related to centered moments has no component with respect to translational motion along x and y. In this study we control 4 DOF of camera motion for planar objects. The set of features that have been used for x, y, and z control are the combination of geometry moments. For orientation control the combination of centered moment has been applied [5], [9]. Similar to [9] the following set of features was chosen:

$$S = (x_n, y_n, a_n, \alpha) \tag{14}$$

where $x_n = x_g a_n$, $y_n = y_g a_n$, $a_n = Z^* \sqrt{a^*/a}$. For controlling the camera velocity in x and y directions, $x_g = \frac{m_{10}}{m_{00}}$ and $y_g = \frac{m_{10}}{m_{00}}$ have been considered, which are the coordinates of the mass center of object. In order to eliminate the effect of scaling, they have been normalized. For controlling the camera in Z direction the area of the object in the image with respect to target image is calculated. Current Z can be calculated by noting that in parallel situation $Z^*\sqrt{a^*} = Z\sqrt{a}$ [9], which a^* is the area and Z^* is the depth of the point with respect to camera in target position. Minimum and maximum of second order moments are used to determine the miner and major of object principal axes respectively. The angle between nearest principal axis to the x axis is determined by

$$\alpha = \frac{1}{2} tan^{-1} \frac{2\mu_{11}}{\mu_{20} - \mu_{02}} \tag{15}$$

The difference between current orientations to target orientation determines the angle of rotation around optical axes. Considering the parallel situation, α is invariant to any translational motions. This formula is only applicable for $\frac{-\pi}{2} \leq \alpha \leq \frac{\pi}{2}$ By utilizing (15), (16), and selected features, the interaction matrix is obtained:

$$L = \begin{bmatrix} -1 & 0 & 0 & Y_n \\ 0 & -1 & 0 & -X_n \\ 0 & 0 & -1 & 0 \\ 0 & 0 & 0 & -1 \end{bmatrix} \tag{16}$$

Because of converting pixel coordinates to the metric coordinates, the off diagonal elements of the matrix are so small that the interaction matrix is so close to diagonal matrix.

III. Control Law

A. Sliding Mode Control Law

In reference [13] the proportional controller has been defined which guarantees limited performance and robustness and it fails to apply in complex situations. In this paper, we propose a first order sliding mode control which is one of the classical approaches to robust control design of uncertain systems. The advantages of proposed method are its robustness to parameter variations and disturbances, and improvement in performance of nonlinear systems.

The control process of image based sliding mode has been illustrated in Fig. 1. in which ω represents joint velocity, and θ is the joint command.

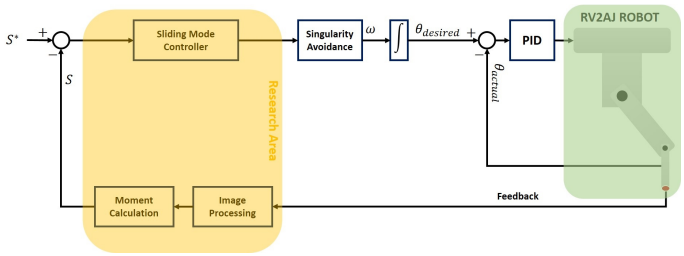

Fig. 1. control diagram

The difference between $\mathbf{S}$ and $\mathbf{S}^*$ are fed into the sliding mode controller. First, the control signals are produced by sliding controllers, and then transformed to joint velocities by singularity avoidance (refer to section IV-A). Finally, target joint positions can be obtained by integrating joint velocities. The internal PID controller sets the joint position with acceptable accuracy. The process terminates when the signal errors reach below the determined threshold.

In order to reduce steady state error, PI type of SMC has been utilized. Consider the sliding surface defined by:

$$\mathbf{S} = \mathbf{e_\xi} + \boldsymbol{\lambda} \int \mathbf{e_\xi} \tag{17}$$

where $\mathbf{e}_\xi$ is the difference between the current feature- measurement and the desired feature-measurement, and λ is the positive arbitrary scalar. The derivative of $\mathbf{S}$ is given by

$$\dot{\mathbf{S}} = \frac{d\mathbf{S}}{dt} = \dot{\mathbf{e}}_{\boldsymbol{\xi}} + \boldsymbol{\lambda}\mathbf{e}_{\boldsymbol{\xi}} \tag{18}$$

The derivative of error signal ($e = \mathbf{s} - \mathbf{s}^*$) is written [13]:

$$\dot{\mathbf{e}} = \dot{\mathbf{s}} = \mathbf{L}_s \mathbf{v}_c \tag{19}$$

by substituting (19) in (18) :

$$\begin{cases} \dot{\mathbf{S}}_\alpha = -\mathbf{v}_{\omega z} + \lambda \mathbf{e}_\alpha \\ \dot{\mathbf{S}}_z = -\mathbf{v}_z + \lambda \mathbf{e}_z \\ \dot{\mathbf{S}}_y = -\mathbf{v}_y - x_n \mathbf{v}_{\omega z} + \lambda \mathbf{e}_y \\ \dot{\mathbf{S}}_x = -\mathbf{v}_x + y_n \mathbf{v}_{\omega z} + \lambda \mathbf{e}_x \end{cases} \tag{20}$$

the control signals are obtained by:

$$\begin{cases} \mathbf{v}_{\omega z} = \lambda e_\alpha + k_\alpha sat(S_\alpha) \\ \mathbf{v}_z = \lambda e_z + k_z sat(S_z) \\ \mathbf{v}_y = \lambda e_y + k_y sat(S_y) \\ \mathbf{v}_x = \lambda e_x + k_x sat(S_x) \end{cases} \tag{21}$$

where sat function is defined by

$$sat(S) = \begin{cases} 1 & \text{if } S > \varphi \\ S/\varphi & \text{if } |S| \leq \varphi \\ -1 & \text{if } S < -\varphi \end{cases} \quad (22)$$

B. Stability Analysis

The lyapunov method has been used for stability analysis. Consider candidate lyapunov function as

$$\mathbf{V} = \frac{1}{2}\mathbf{S}^2 \quad (23)$$

From (23) the derivative of V, may be computed as $\dot{V} = S\dot{S}$ which should be negative definite to assure stable control law. Considering $sign$ function instead of sat function in equation (21), and substituting in (20), $\dot{S}$ is given by

$$\dot{S} = -Ksign(S) \quad (24)$$

where K is positive definite and it should be specified by sliding condition. When S is positive, the $\dot{S}$ is negative and vice versa, consequently $\dot{V}$ is negative definite. Using sat function (defined by (22)), reaching time to sliding surface boundary is given by

$$t_r = \frac{|S(0)| - \varphi}{K} \quad (25)$$

In the boundary layer the derivative of S is defined by

$$\dot{S} = -K\frac{S(t)}{\varphi} \quad (26)$$

The solution of differential equation (26) is defined by:

$$S(t) = \varphi sign[S(t_r)]e^{-\frac{K}{\varphi}(t - t_r)} \quad (27)$$

which shows sliding surface decreases exponentially [14].

IV. Experimental Results

To validate the proposed controller, several experiments have been performed using a 5-DOF RV-2AJ industrial manipulator, with one degree of redundancy in manipulator's y direction made by gantry . A camera has been mounted on the manipulator's end effector. Fig. 2 shows the Experimental setup. Camera has been equipped with a wide lens with 2.1 mm focal length, and provides images with 30 fps rate, and resolution of 320x240. The moments are computed on the binary images in metric coordinates. Target joints are computed and sent to robot using a 1.84-GHz CPU and 2 GB RAM computer. OpenCV library has been used for required image processing. The control algorithm has been developed in visual studio 2008 environment. Although all image capturing, image processing, and control signal calculation were handled through multithread programming with a run time of every 10 ms, in practice the limited sampling rate of camera imposed sampling time of around 33 ms.

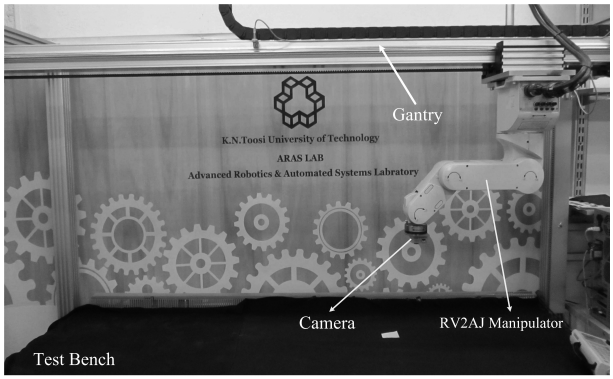

Fig. 2. RV2AJ manipulator configuration

A. Empirical Considerations

VS is performed at a number of discrete points in space. 5 degree of manipulator has many singular points that are not reachable directly. Thanks to the one degree redundancy of gantry robot, the trajectories toward target points may be chosen far from singular configuration. The controller of manipulator and gantry are not integrated. The accuracy of robot is about 0.02 mm and the accuracy of gantry is about 1mm. Therefore in the large displacement the motion of gantry increases the error in y direction slightly. The wide lens has radial distortion which causes an outward displacement between given image points and their ideal locations. The removal of the radial distortion has been performed by estimating the distortion coefficients in camera calibration matlab toolbox [15]. These coefficients are used by OpenCV undistort function to correct distortion. The provided image from undistort function, has been binarized by threshold algorithm. it is worth to mention that the large threshold value causes the loss of information, while the smaller value, results in noisy image. Several approaches for threshold level selection have been proposed in [16], however here it has been chosen by experiments. In the controller, for avoiding wind up problem of the integrator, λ has been chosen sufficiently small. For all the experiments K, λ, and φ have been adjusted empirically as $\lambda_x = \lambda_y = 0.001$, $\lambda_z = \lambda_\alpha = 0.003$, $K_x = 80$, $K_y = 100$, $K_z = 70$, $K_\alpha = 3$, and $\varphi_x = \varphi_y = \varphi_z = 0.03$, and $\varphi_\alpha = 0.06$. The algorithm terminates when the feature errors are below 0.001 for 10 iterations.

B. Case of a simple Nonsymmetrical Object

In this section, the Moment based sliding mode VS is compared to the kernel based sliding mode VS. For better comparison, the difference between initial and target position has been chosen close to the experiments in [1] and has been repeated 8 times for different initial positions. The results of a set of experiments are graphed in Figs. 3. Fig.3(e) illustrates negligible oscillations of the control signal after about 15 iterations. The small oscillations of the control signal arises from eliminating the chattering phenomenon in the sliding mode by utilizing sat function. In Fig. 3(d) the

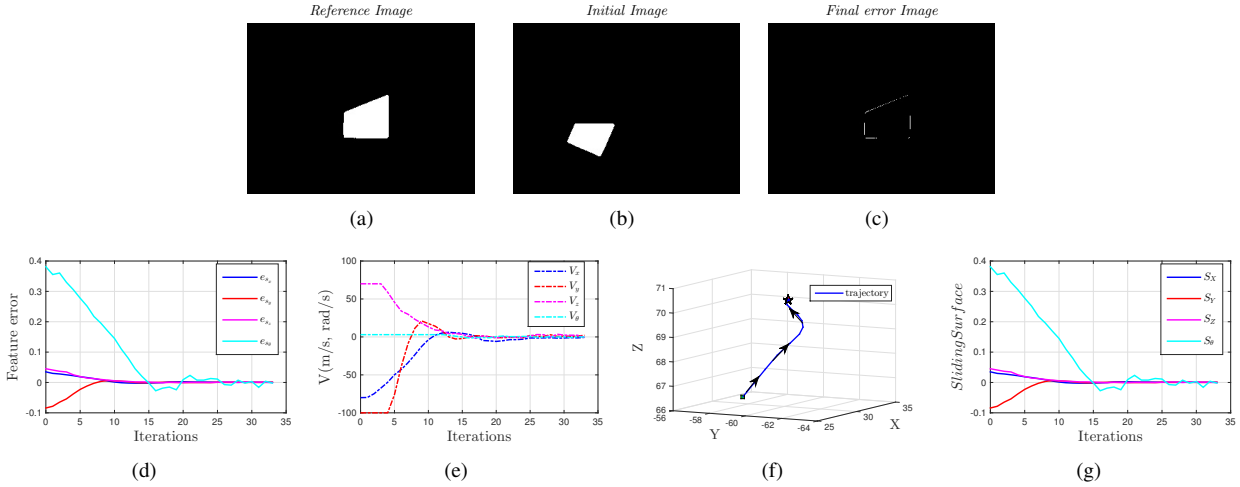

Fig. 3. Experimental Results 1. (a) Desired Image. (b) Initial Image. (c) Difference between final Image and Desired Image. (d) Moment Errors. (e) Robot Velocities. (f) Camera 3D Trajectory. (g) Sliding surface

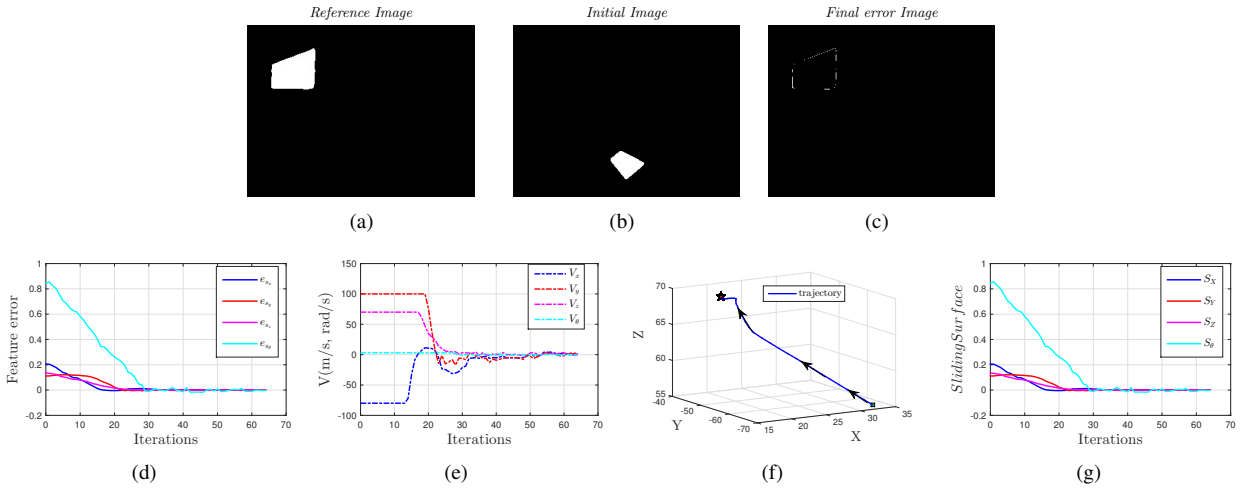

Fig. 4. Experimental Results 2. (a) Desired Image. (b) Initial Image. (c) Difference between final Image and Desired Image. (d) Moment Errors. (e) Robot Velocities. (f) Camera 3D Trajectory. (g) Sliding surface

exponential reduction of errors can be seen. In Fig. 3(f), the spatial trajectory of end effector has been displayed; the initial position and the target position have been indicated by point and star respectively. Although the interaction matrix is updated at each iteration, the trajectory is not straight duo to singularity avoidance function effect. The performance of the proposed method on the set of experiments is in contrast to the kernel approach as compared in table I and II. The error mean in all directions have decreased considerably. In x, and α directions mean error has decreased 8 times. in y and z directions mean error has decreased 14 and 89 times respectively. The considerable decrease of error in z and α direction compared to the kernel based method comes from decoupled features and simultaneous control of 4 DOF camera motion.

In order to evaluate the performance of proposed method, the farther initial position from target position has been tested. The results of such experiments are illustrated in Fig.4 which

TABLE I
KERNEL BASED SLIDING MODE VS ERRORS IN 4D

Pose error	Initial condition		Final error	
	Mean	Std.	Mean	Std.
ex, (mm)	45.0	12.3	3.1	3.1
ey, (mm)	41.3	10.9	8.5	9.4
ez, (mm)	44.6	0.3	13.3	4.0
eθ, (degree)	25	12.91	1.26	0.62

are the verification to increase of domain of attraction with respect to KBSMVS.

Statistical ranges of tests have been summarized in table III. In the second set of experiments, although the distance increased more than 2 times, the error mean in x, y, z, and α direction have decreased 3 times, 7 times, 17 times, and 4 times respectively. we observed significant improvements in camera trajectory, accuracy, and time of convergence.

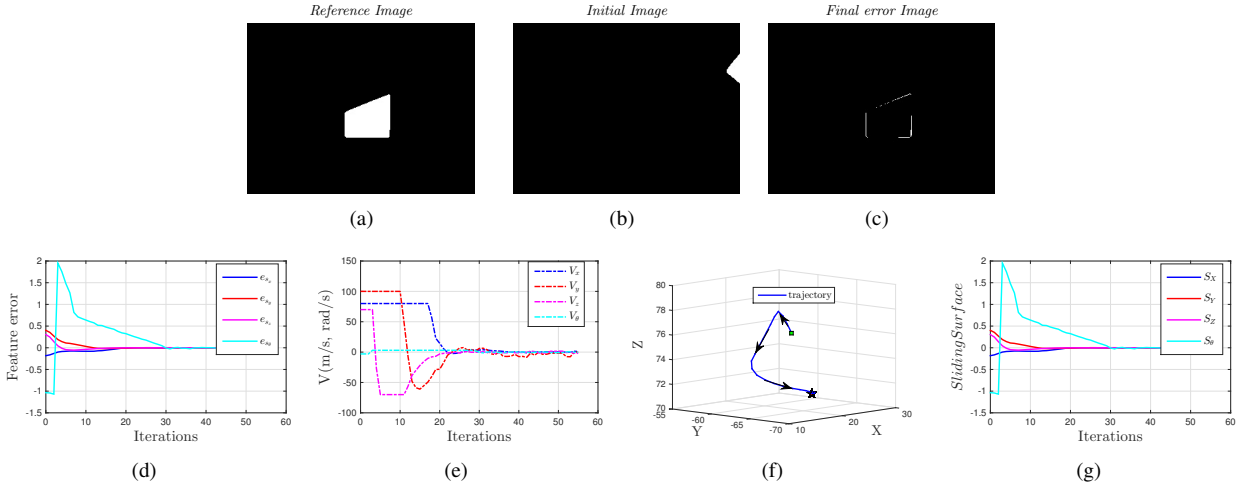

Fig. 5. Experimental Results 3. (a) Desired Image. (b) Initial Image. (c) Difference between final Image and Desired Image. (d) Moment Errors. (e) Robot Velocities. (f) Camera 3D Trajectory. (g) Sliding surface

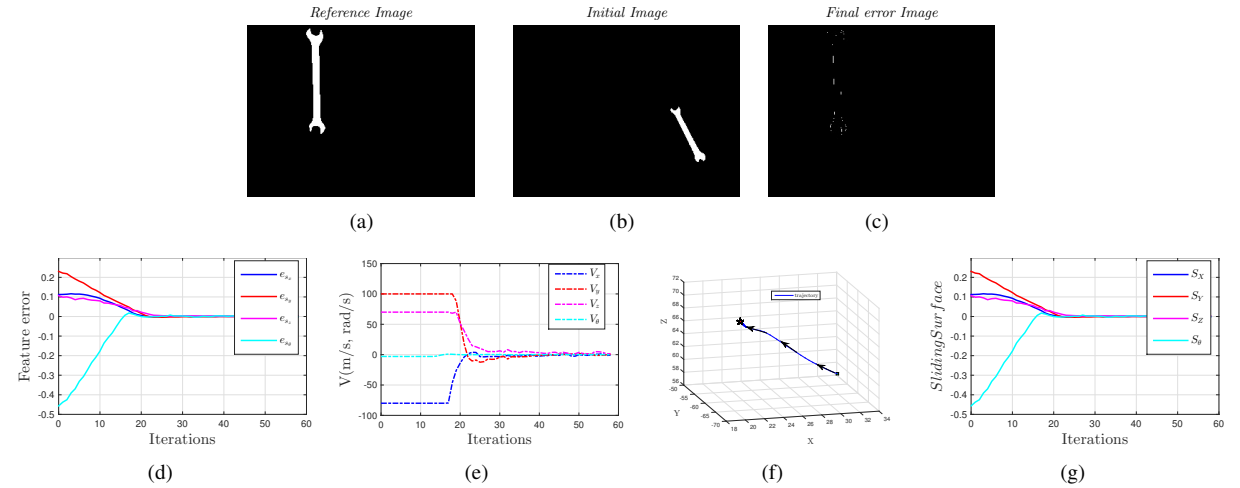

Fig. 6. Experimental Results 4. (a) Desired Image. (b) Initial Image. (c) Difference between final Image and Desired Image. (d) Moment Errors. (e) Robot Velocities. (f) Camera 3D Trajectory. (g) Sliding surface

TABLE II
MOMENT BASED SLIDING MODE VS ERRORS IN 4D

Pose error	Initial condition		Final error	
	Mean	Std.	Mean	Std.
ex, (mm)	44.23	2.88	0.39	0.45
ey, (mm)	44.08	8.08	0.61	0.43
ez, (mm)	47.22	2.72	0.15	0.34
eθ, (degree)	23.28	0.69	0.15	0.25

TABLE III
FINAL ERROR RESULTS OF MBSMVS FOR LARGER DISPLACEMENT

Pose error	Initial condition		Final error	
	Mean	Std.	Mean	Std.
ex, (mm)	132.37	12.87	0.99	0.43
ey, (mm)	190.24	42.41	1.24	0.83
ez, (mm)	135.69	20.09	0.77	0.65
eθ, (degree)	50.78	1.00	0.30	0.14

C. Case of the extraneous image regions

In this section, classical control method is compared to the proposed sliding mode control. In the case of extraneous image regions there is an unmodeled disturbance to the system. The uncertainty in error due to disappearance of some portions of scene from the camera field of view prevents the convergence of the classical control. Thanks to the sliding mode control robustness, this uncertainty can be handled. Different experiments have been done to examine the robustness of proposed method to partial disappearance of scene. In Fig. 5 the results have been illustrated. In Fig 5(b) the initial condition with partial appearance of the object is displayed and in Fig. 5(c) the final error can be seen. Disappearance of features affects the calculation of the area and angle of rotation and results in wrong detection of error in z and α directions. After about 3 iterations, the control signal in x and

y directions modify the position of camera partially and make it possible to detect the complete shape of the object. Then the controller flips the signs in z and α directions immediately to modify the camera trajectory. In 3D camera trajectory this issue completely observable, too. The accuracy of method have been compared to the results of previous section. 8 different experiments have been done to verify the robustness of method and the results are summarized in Table. IV. Although the error mean increased compared to the previous section, they are smaller than the results of kernel based sliding mode shown in Table. I. In order to validate the robustness, different objects

TABLE IV
MBSVS ERRORS IN EXTRANEOUS REGIONS 4D

Pose error	Initial condition		Final error	
	Mean	Std.	Mean	Std.
ex, (mm)	125.78	36.31	1.54	0.39
ey, (mm)	179.18	32.95	0.52	0.86
ez, (mm)	58.42	58.09	0.60	0.37
eθ, (degree)	22.50	7.69	0.29	0.22

were examined. Here a wrench has been tested. Because of its material, it has reflection, as a result during camera trajectory some parts of it are disappeared. The results of 8 experiment with different initial points have been summarized in Table. V. The initial points, except in α direction, are selected close to second experiment. Compared to the results of second set of experiments the mean error in x, y, and z direction has been increased 3, 2, 8 times respectively because of unplanar shape of the object.

TABLE V
MBSVS ERRORS FOR UNPLANAR REAL OBJECT

Pose error	Initial condition		Final error	
	Mean	Std.	Mean	Std.
ex, (mm)	134.81	15.55	1.35	1.14
ey, (mm)	175.20	32.65	1.13	0.81
ez, (mm)	135.54	20.02	1.14	1.09
eθ, (degree)	48.28	7.54	0.09	0.04

V. CONCLUSION

This paper applies a robust nonlinear controller to the moment-based visual servoing. The combination of sliding mode controller with visual servoing, which has inherent nonlinear dynamics, leads to better results. The assigned controller achieves a large domain of attraction. In addition, its performance in the sense of accuracy, and time of convergence has improved compared to kernel-based sliding mode. This controller looks promising for other method of visual servoing.

REFERENCES

[1] M. Parsapour and H. D. Taghirad, "Kernel-based sliding mode control for visual servoing system," *IET Computer Vision*, vol. 9, no. 3, pp. 309–320, 2014.

[2] B. Espiau, F. Chaumette, and P. Rives, "A new approach to visual servoing in robotics," *Robotics and Automation, IEEE Transactions on*, vol. 8, no. 3, pp. 313–326, 1992.

[3] S. Hutchinson, G. D. Hager, P. Corke *et al.*, "A tutorial on visual servo control," *Robotics and Automation, IEEE Transactions on*, vol. 12, no. 5, pp. 651–670, 1996.

[4] K. Deguchi, "A direct interpretation of dynamic images with camera and object motions for vision guided robot control," *International Journal of Computer Vision*, vol. 37, no. 1, pp. 7–20, 2000.

[5] F. Chaumette, "Image moments: a general and useful set of features for visual servoing," *Robotics, IEEE Transactions on*, vol. 20, no. 4, pp. 713–723, 2004.

[6] M. Sonka, V. Hlavac, and R. Boyle, *Image processing, analysis, and machine vision*. Cengage Learning, 2014.

[7] A. G. Mamistvalov, "N-dimensional moment invariants and conceptual mathematical theory of recognition n-dimensional solids," *Pattern Analysis and Machine Intelligence, IEEE Transactions on*, vol. 20, no. 8, pp. 819–831, 1998.

[8] S. Reddi, "Radial and angular moment invariants for image identification," *IEEE Transactions on Pattern Analysis & Machine Intelligence*, no. 2, pp. 240–242, 1981.

[9] O. Tahri and F. Chaumette, "Point-based and region-based image moments for visual servoing of planar objects," *Robotics, IEEE Transactions on*, vol. 21, no. 6, pp. 1116–1127, 2005.

[10] M. Bakthavatchalam, F. Chaumette, and O. Tahri, "An improved modelling scheme for photometric moments with inclusion of spatial weights for visual servoing with partial appearance/disappearance," in *IEEE Int. Conf. on Robotics and Automation, ICRA'15*, 2015.

[11] V. Kallem, M. Dewan, J. P. Swensen, G. D. Hager, and N. J. Cowan, "Kernel-based visual servoing," in *Intelligent Robots and Systems, 2007. IROS 2007. IEEE/RSJ International Conference on*. IEEE, 2007, pp. 1975–1980.

[12] A. K. Jain, *Fundamentals of digital image processing*. Prentice-Hall, Inc., 1989.

[13] F. Chaumette and S. Hutchinson, "Visual servo control. i. basic approaches," *Robotics & Automation Magazine, IEEE*, vol. 13, no. 4, pp. 82–90, 2006.

[14] S. M. Mahmoud, L. Chrifi-Alaoui, V. Van Assche, and P. Bussy, "Sliding mode control of nonlinear siso systems with both matched and unmatched disturbances," *Proc. International Journal on Sciences and Techniques of Automatic control, IJ-STA*, vol. 2, no. 1, pp. 350–367, 2008.

[15] "MS Windows NT camera calibration," http://www.vision.caltech.edu/bouguetj/calib_doc/, 2015, accessed: 2015-07-03.

[16] R. C. Gonzalez, *Digital image processing*. Pearson Education India, 2009.